Geophysical Prospecting EAGE EUROPEAN ASSOCIATION OF GEOSCIENTISTS & ENGINEERS

Geophysical Prospecting, 2012, **60**, 444–465 doi: 10.1111/j.1365-2478.2011.01011.x

Wave-equation migration with dithered plane waves

Francesco Perrone* and Paul Sava

Center for Wave Phenomena, Department of Geophysics, Colorado School of Mines, 1500 Illinois Street, Golden, CO 80401, USA

Received March 2010, revision accepted July 2011

ABSTRACT

Wave-equation based shot-record migration provides accurate images but is computationally expensive because every shot must be migrated separately. Shot-encoding migration, such as random shot-encoding or plane-wave migration, aims to reduce the computational cost of the imaging process by combining the original data into synthesized common-source gathers. Random shot-encoding migration and plane-wave migration have different and complementary features: the first recovers the full spatial bandwidth of the image but introduces strong artefacts, which are due to the interference between the different shot wavefields; the second provides an image with limited spatial detail but is free of crosstalk noise. We design a hybrid scheme that combines linear and random shot-encoding in order to limit the drawbacks and merge the advantages of these two techniques. We advocate mixed shot-encoding migration through dithering of plane waves. This approach reduces the crosstalk noise relative to random shot-encoding migration and increases the spatial bandwidth relative to conventional plane-wave migration when the take-off angle is limited to reduce the duration of the plane-wave gather. In turn, this decreases the migration cost. Migration with dithered plane waves operates as a hybrid encoding scheme in-between the end members represented by plane-wave migration and random shot-encoding. Migration with dithered plane waves has several advantages: every synthesized common-source gather images in a larger aperture, the crosstalk noise is limited and higher spatial resolution is achievable compared to shot-record migration, random shot-encoding and linear shot-encoding, respectively. Computational cost is also reduced relative to both random and linear shot-encoding migration since fewer synthesized common-source gathers are necessary to obtain a high signal-to-noise ratio and high spatial resolution in the final image.

Key words: Artefacts, Shot-encoding, Wave-equation migration.

1 INTRODUCTION

The data used in seimic imaging are acquired by means of independent experiments that are then separately imaged. In wave-equation migration, the imaging procedure consists of two steps: the wavefield extrapolation, from data recorded on the surface to all locations in the subsurface and the application of an imaging condition (Claerbout 1985). The extrapolation step is linear but computationally intensive; the imaging step is relatively cheap from a computational point of view but non-linear. The imaging condition extracts an image where the data, extrapolated backward in time, match the source wavefield, extrapolated forward in time. A conventional imaging condition evaluates the matching between the source and receiver wavefields through their crosscorrelation (Claerbout 1985).

*E-mail: fperrone@mymail.mines.edu

© 2011 European Association of Geoscientists & Engineers

In shot-record (shot-profile) migration, every experiment is imaged separately and the total cost is therefore a linear function of the number of experiments. Moreover, the more accurate the wavefield extrapolation scheme, the higher its computational cost. In the case of reverse-time migration (Baysal, Kosloff and Sherwood 1983; McMechan 1983), the computational cost is high, thus posing a challenge for industrial applications. Simultaneous shot migration has several benefits: first, we can reduce the overall time of the migration procedure, thus reducing the cost; second, we can exploit the possibility of imaging in a fixed time and in a bigger aperture compared to shot-profile migration in the migration velocity analysis loop, which is a crucial step in the seismic inversion process.

Random shot-encoding migration (Morton and Ober 1998; Romero *et al.* 2000; Cazzola *et al.* 2004) is used to image data by simultaneously migrating a number of shots, which are linearly combined after the application of random delays. The main goal is to reduce the computational cost of wave-equation migration. The drawback is that unrelated shots interfere with one another, thus leading to artefacts commonly referred to as crosstalk. For random shot-encoding, the amplitude of the artefacts in the image decreases as $1/\sqrt{M}$ with M being the number of encodings considered, i.e., the number of stacked encoded images.

An intrinsic problem in shot-profile migration is that the natural prestack gather (the shot indexed gather) cannot be directly or easily related to the incidence angle or other illumination-related quantities (Soubaras 2006). To overcome this difficulty, several authors propose synthesizing composite shots by applying delays that are linear functions in the original shot positions (Whitmore 1995; Zhang *et al.* 2005; Liu *et al.* 2006). These new synthesized shots are synthetic plane waves and the new data are, therefore, the response of the subsurface to an incident plane wave. The natural prestack index for these experiments is the ray parameter $\mathbf{p}$, which is a surface-related parameter and does not remove the complexity of the overburden at the image point, i.e., it does not represent the illumination of the image point as a function of the angle of incidence.

The angle of incidence represents a preferential domain for indexing seismic images. Plane-wave migration produces images that can be indexed using the ray-parameter or take-off angle, which is directly related to the angle of incidence in depth only if the velocity model is layered and laterally homogeneous. In complex velocity models, the angle of incidence can be computed by using extended images and transforming them into the angle domain (Rickett and Sava 2002; Sava and Fomel 2003). Nonetheless, plane-wave migration is a particular instance of shot-profile migration and can produce kinematic artefacts in strongly refracting models for each individual migrated image (Stolk and Symes 2004).

Plane-wave migration, or linear shot-encoding migration, is equivalent to shot-profile migration when one considers all plane waves that describe the data. Zhang *et al.* (2005) presented an equation for the minimum number of plane-wave components necessary for correctly representing the data in a certain range of take-off angles. Soubaras (2006) presented a different strategy that exploits a unitary transformation for combining the original shots. Modulated shot-encoding produces an image equivalent to shot-profile migration as well as image-gathers indexed by ray parameter $\mathbf{p}$ but it is less costly than plane-wave migration. Modulated shot-encoding and plane-wave migration are closely related: both combine the shots through a unitary transformation but while modulated shot-encoding uses a frequency independent unitary transformation, plane-wave migration uses a frequency dependent basis. They span the same frequency-wavenumber space $(\omega, \mathbf{p})$ but in different ways. The modulated shot-encoding algorithm represents an improvement over both plane-wave migration and shot-record migration and the computational gain is preserved in the time-domain implementation (Zhang, Sun and Gray 2007). In this work, we present an alternative algorithm, suitable for reverse-time migration, which allows straightforward implementation, quality control of the final image and computational cost reduction.

The artefacts produced in simultaneous migration of different shots originate in the migration operator. The migration operator (wavefield extrapolation followed by the application of an imaging condition) is simply the adjoint of the forward Born operator used for modelling the data (Lailly 1983). This operator is 'almost' unitary when all experiments are individually migrated and the results are then stacked together. For simultaneous shot migration, the migration operator is no longer unitary, which is evidenced by the artefacts that contaminate the image. An alternative approach to this problem is least-squares migration; in this way we can compensate for the non-unitary nature of the migration operator and eliminate the artefacts in the image (Tang and Biondi 2009). Least-squares migration is effective but computationally expensive: shot-encoding is intended to reduce the computational cost but a least-squares inversion of such a large linear problem makes the process less cost-effective. It is interesting to observe the similarities between the least-squares approach to

simultaneous shot migration and processing of blended data (Berkhout 2008), where datasets with overlapping shots are processed and imaged in a least-square sense (Verschuur and Berkhout 2009; Berkhout, Verschuur and Blacquière 2009).

In this paper, we analyse shot-encoding schemes, namely random shot-encoding ((Romero *et al.* 2000) and plane-wave migration (Zhang *et al.* 2005), which are suitable for reverse-time migration. We look at the behaviour of the two methods with respect to crosstalk artefacts and spatial resolution in the final image. Our goal is to develop an improvement over random shot-encoding that converges faster to the shot-record migration result and controls the artefacts introduced in the image by the interference of different experiments. At the same time, we want to achieve higher spatial resolution compared to plane-wave migration when we limit the take-off angle range, which trades speed for spatial resolution by using only certain plane-wave components for reconstructing the image of the subsurface. Moreover, when a time-domain finite difference scheme is used (like in reverse-time migration), imaging plane-wave components with a high take-off angle (or ray parameter **p**), requires an increase in the computational time and cost since long delays have to be taken into account. From this analysis, we design a hybrid encoding scheme that combines linear and random shot-encoding migration. First, we construct the linear delay function that produces the synthetic plane-wave response from the original data; then, we dither the planar wavefront with random delays in order to increase the spatial resolution without migrating additional plane waves. We test it on the synthetic Sigsbee model and show that it is more effective than both linear and random shot-encoding migration. In areas with poor or uneven illumination, the hybrid approach is less prone to crosstalk noise than random shot-encoding migration and recovers the full spatial bandwidth of the image that is available in the data, in contrast to linear shot-encoding migration when a limited range of take-off angles is considered.

2 SHOT-ENCODING METHODS

The imaging condition is a non-linear operation; it is not able to distinguish between wavefields from different shots and produces artefacts when several experiments are simultaneously migrated. Let us consider the source wavefields $s_i(\mathbf{x}, t)$ and the receiver wavefields $r_i(\mathbf{x}, t)$, where the index i indicates the shot number and $\mathbf{x} = (x, y, z)$ represents the position vector. In shot-record migration the image for a single shot $I_i(\mathbf{x})$ is computed as the cross-correlation at time lag $\tau = 0$ of the source and receiver wavefields at every location $\mathbf{x}$:

$$I_i(\mathbf{x}) = \sum_t s_i(\mathbf{x}, t) r_i(\mathbf{x}, t). \tag{1}$$

Since the wave equation we use is linear in the wavefields, we can combine wavefields of different shots and extrapolate them all at once; however, problems arise in the extraction of the image. If we consider the new source wavefield $S(\mathbf{x}, t) = \sum_i s_i(\mathbf{x}, t - \tau_i)$ and receiver wavefield $R(\mathbf{x}, t) = \sum_i r_i(\mathbf{x}, t - \tau_i)$, which are linear combinations of the source and receiver wavefields of all shots with different time delays, we can still extract an image computing:

$$I(\mathbf{x}) = \sum_t S(\mathbf{x}, t) R(\mathbf{x}, t). \tag{2}$$

Substituting the expressions for the synthesized source and receiver wavefields, we obtain:

$$I(\mathbf{x}) = \sum_t \sum_i \sum_j s_i(\mathbf{x}, t - \tau_i) r_j(\mathbf{x}, t - \tau_j) \tag{3}$$

$$= \sum_i I_i(\mathbf{x}) + \sum_t \sum_{k \neq l} s_k(\mathbf{x}, t - \tau_k) r_l(\mathbf{x}, t - \tau_l), \tag{4}$$

where $I_i(\mathbf{x})$ is the image obtained from the ith shot (equation (2)), and the term $\sum_t \sum_{k \neq l} s_k(\mathbf{x}, t - \tau_k) r_l(\mathbf{x}, t - \tau_l)$ represents the crosstalk artefacts produced by the imaging condition as the result of the simultaneous migration of different experiments. Shot-encoding migration involves the design of an optimal combination of the original data, which allows one to simultaneously migrate several shots at once, control the crosstalk noise and recover the correct image of the structure that generated the recorded data.

Different encoding schemes have been discussed in the literature. Random shot-encoding (Morton and Ober 1998; Romero *et al.* 2000) and linear shot-encoding (Whitmore 1995; Zhang *et al.* 2005) apply simple delays to the source and receiver wavefields of every shot. In random shot-encoding, a random delay is applied to each one of the shot wavefields prior to the composition of the synthetic experiments. The non-correlation of the delays is reflected in uncorrelated artefacts that can be stacked out by summing up the images obtained from different realizations of random delays.

On the other hand, linear shot-encoding aims to construct the response of the Earth to synthetic plane waves by applying delays that are linear functions of the shot positions. Linear shot-encoding migration has been proven to be equivalent to shot-record migration if a sufficient number of plane waves is considered. Random shot-encoding is equivalent to shot-record migration when considering an infinite number of

realizations of random delays. For both methods, because of the model-dependence of the problem, the question of how many encodings we really need for obtaining an image equivalent to the shot-profile migration result is still open (Stork and Kapoor 2004; Etgen 2005). For example, for imaging a single horizontal reflector, we need a single plane wave; in contrast, for highly heterogeneous media and complex structures, a more complete illumination of the spatial wavenumber domain is required. In the latter case, random shot-encoding can represent a more economic solution, given an acceptable level of crosstalk.

A third encoding scheme that involves more than just simple delays is modulated shot-encoding (Soubaras 2006) or, in the time-domain implementation, harmonic-source encoding (Zhang *et al.* 2007). These strategies are effective but not straightforward to implement, especially the time-domain implementation. Harmonic-source encoding involves the convolution of the original data with a filter that decays like $1/t$ and particular care is needed in the choice of the encoding parameters. Nonetheless, both methods halve the computational cost of a typical production project (Soubaras 2006; Zhang *et al.* 2007).

Our work aims to find a simple and economic way to image a survey using reverse-time migration. We focus on random and linear shot-encoding migration and all considerations are drawn from these two references and their features compared to the standard shot-profile migration.

Both random and linear shot-encoding can be described using a general formulation of the encoding procedure. In fact, we can express the synthetic wavefields as a weighted sum of the actual shot wavefields appropriately delayed:

$$S(\mathbf{x}, t, \eta) = \sum_k s_k(\mathbf{x}, t) * \delta(t - f(\mathbf{x}_k, \eta)) \tag{5}$$

and

$$R(\mathbf{x}, t, \eta) = \sum_k r_k(\mathbf{x}, t) * \delta(t - f(\mathbf{x}_k, \eta)), \tag{6}$$

where $f(\mathbf{x}_k, \eta)$ represents the delay applied to the kth shot wavefields as a function of the shot position $\mathbf{x}_k$ and the parameter η, and the function $\delta(t - f(\mathbf{x}_k, \eta))$ is the Dirac delta function centred at $t = f(\mathbf{x}_k, \eta)$ and $*$ denotes convolution. The parameter η spans the encoding axis. For example, in the case of plane-wave migration in a 2D model (Whitmore 1995; Zhang *et al.* 2005), we have

$$f(x_k, \eta) = \frac{\sin(\alpha\eta)}{v}(x_k - x_0), \tag{7}$$

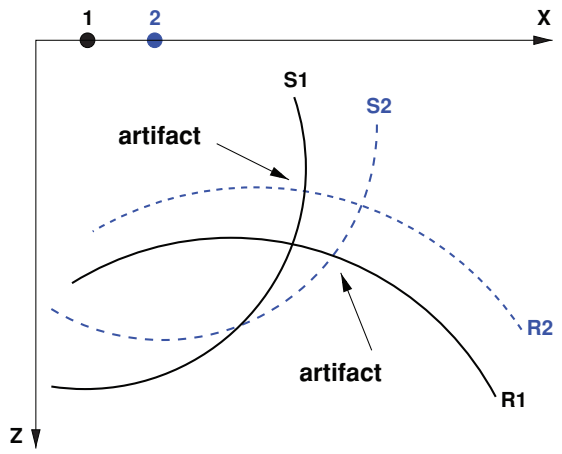


Figure 1 Artefacts generated by the imaging condition: the wavefields corresponding to different shots are represented with different colours and different lines and indicated with numbers 1 and 2. The source wavefields are S1 and S2, the receiver wavefields R1 and R2. The correct image is produced where the wavefields of the same shots coincide, i.e., where the two solid lines, S1 and R1 and the two dashed lines, S2 and R2, intersect. Shot-encoding migration generates artefacts where S1 intersects R2 and S2 intersects R1.

where x_0 is a reference point, v is the phase velocity and $\alpha\eta$ represents the take-off angle of a single plane wave; for random shot-encoding, $f(\mathbf{x}_k, \eta)$ is a random process with different values for every shot position $\mathbf{x}_k$, where the parameter η indexes the random delay realizations.

If N represents the total number of shots and M the number of different encodings (plane waves or random delay realizations), the strategy is effective if $M \ll N$, i.e., if we can obtain an image that is comparable in quality to shot-record migration with a smaller number of migrations.

The wave-equation used in seismic imaging is linear in the wavefield; hence, we can linearly combine wavefields of different shots and numerically propagate their superposition in the subsurface model. However, the imaging condition is a non-linear operation and introduces crosstalk between different experiments. The cartoon in Fig. 1 describes the mechanism that produces crosstalk when two shots are simultaneously migrated. When the source and receiver wavefields belonging to different experiments match in time, the imaging condition extracts an image that does not correspond to a reflection.

If we insert the expressions for the synthetic wavefields (equations 5 and 6) into the imaging condition in equation (2) and then transform it into the frequency domain, we obtain

$$I(\mathbf{x}) = \sum_\omega \sum_k \sum_l s_k(\mathbf{x}, \omega) r_l^*(\mathbf{x}, \omega) W_{kl}, \tag{8}$$

where

$$W_{kl} = \sum_{\eta} \exp^{i\omega[f(\mathbf{x}_l,\eta) - f(\mathbf{x}_k,\eta)]}. \quad (9)$$

The matrix W_{kl}, which has the shot positions $\mathbf{x}_l$ and $\mathbf{x}_k$ as rows and columns, represents the coupling between different shots in equation (8) and it is fully determined by the encoding function f.

An encoding scheme is considered equivalent to shot-record migration if the crosstalk term in equation (8) approximates the identity matrix, i.e., if the following condition is satisfied:

$$W_{kl} = \sum_{\eta} \exp^{i\omega[f(\mathbf{x}_l,\eta) - f(\mathbf{x}_k,\eta)]} \approx \delta_{kl}, \quad (10)$$

where δ_{kl} is the Kronecker symbol.

In the following sections, we study the crosstalk term for linear shot-encoding and random shot-encoding. We highlight the main features in terms of the spatial bandwidth achievable in the final image and crosstalk noise and then we design a strategy for combining the advantages and limiting the drawbacks of these two schemes. We recognize linear shot-encoding and random shot-encoding as end members of a more general family of encodings, which we can span by controlling the correlation of the delays of neighbouring shots. Figure 2 describes our idea: fixing the computational cost, we can move from plane-wave migration to random shot-encoding, i.e., from low crosstalk and low spatial bandwidth to high crosstalk and high spatial resolution in the final image.

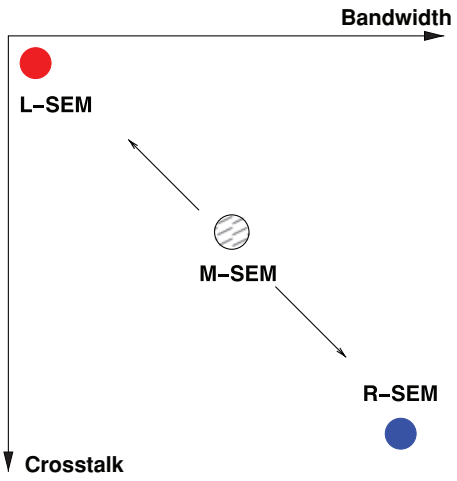


Figure 2 Trade-off between bandwidth and crosstalk for different shot-encoding schemes. Linear shot-encoding migration achieves a clean image with low spatial resolution, while randon shot-encoding migration obtains a full bandwidth image highly contaminated by crosstalk noise. For drawing the cartoon, we assume a fixed computational cost.

The correlation of the delays of neighbouring shots involves a tuning parameter that controls the dithering of an initial plane wave. In Fig. 3, we show the source wavefield for linear shot-encoding, random shot-encoding and a combination of the two, in which the initial plane wave is dithered by a random perturbation. In the following, we analyse linear and random shot-encoding migration and introduce mixed shot-encoding migration as their combination.

2.1 Linear shot-encoding migration

In linear shot-encoding, the recorded wavefields of different experiments are combined in order to obtain the response to a synthetic plane wave. The encoding function is linear in the shot position and depends on one parameter, which represents the ray parameter $\mathbf{p}_\eta$ associated with a particular plane wave:

$$f(\mathbf{x}_k, \eta) = \mathbf{p}_\eta \cdot (\mathbf{x}_k - \mathbf{x}_0), \quad (11)$$

where $\mathbf{x}_0$ represents an arbitrary reference point. Substituting equation (11) into equation (9), we obtain

$$W_{kl} = \sum_{\eta} \exp^{i\omega \mathbf{p}_\eta \cdot (\mathbf{x}_k - \mathbf{x}_l)}. \quad (12)$$

Equation (12) represents a Dirac comb (Oppenheim and Schafer 1999) and tells us that if the $\mathbf{p}$ dimension is properly sampled, the final image will be identical to the shot-record migration result. Several papers discuss the sampling requirements for the $\mathbf{p}$-space (Stork and Kapoor 2004; Zhang *et al.* 2005; Etgen 2005). The take-off angle range constrains the minimum number of plane waves necessary for correctly reconstructing the data in this range. At the same time, the angle range defines the computational cost for reverse-time migration and the accuracy of the image reconstruction and reducing the angle range decreases not only the computational cost but also the quality of the final image. If we assume that the ray parameter space is properly sampled and the synthesized plane waves are not aliased, then equation (12) represents a sinc function (the Discrete Fourier Transform (DFT) of a discrete boxcar function) and tends to a delta function if we increase the take-off angle range.

We can display the crosstalk matrix for a given number of plane waves and analyse the behaviour as a function of the number of $\mathbf{p}$ components considered. In Fig. 4, we observe how the crosstalk term becomes more spikier by imaging more plane-wave components. This is because, for linear shot-encoding, the crosstalk term is actually an approximate representation of the identity operator.

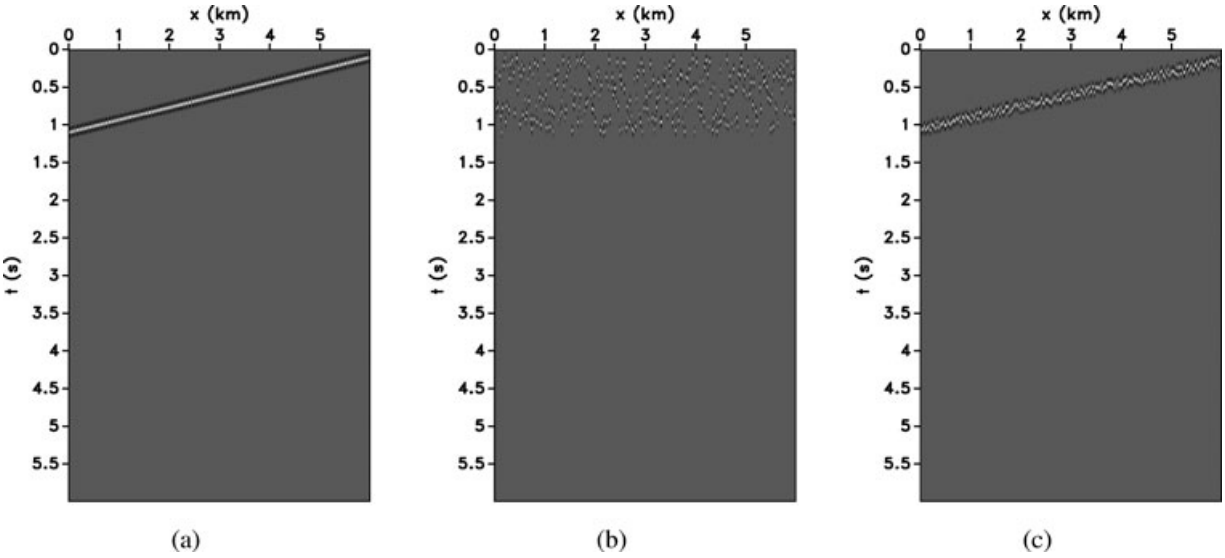


Figure 3 Examples of source wavefield for (a) linear shot-encoding migration, (b) random shot-encoding migration and (c) mixed shot-encoding migration. Mixed shot-encoding consists in dithering the wavefront we synthesize for linear shot-encoding migration.

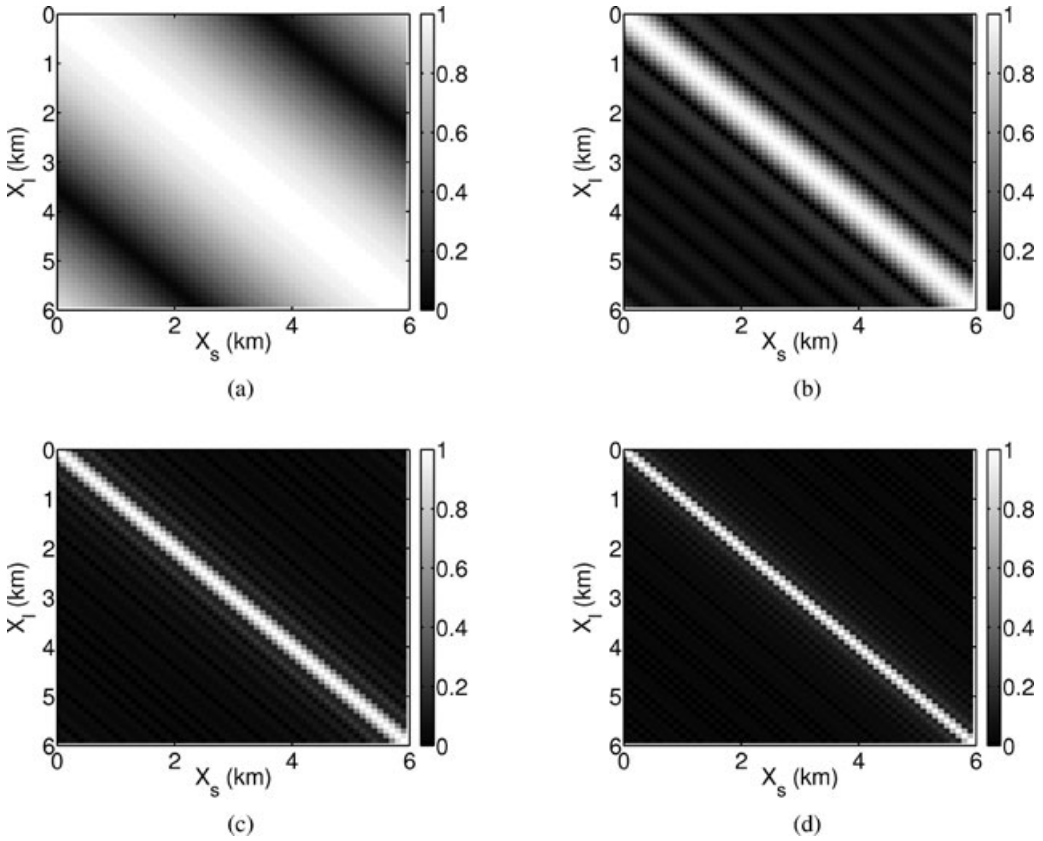


Figure 4 Linear shot-encoding migration crosstalk matrix versus number of plane waves for a single temporal frequency ω: (a) 2, (b) 10, (c) 20 and (d) 30. Increasing the number of plane waves, we sharpen the main diagonal of the crosstalk matrix and better approximate the identity, i.e., we tend toward the shot-record migration result. The coordinates X_l and X_s represent the shot positions. In the case of shot-record migration, the crosstalk matrix is the identity because every shot is considered separately.

2.2 Random shot-encoding migration

In random shot-encoding, the delay for every shot is drawn from a random process and parameter η is the realization index. We use the following notation:

$$f(\mathbf{x}_k, \eta) \sim \mathcal{U}(0, t_{max}; \eta). \tag{13}$$

At every shot location $\mathbf{x}_k$, the delay $f(\mathbf{x}_k, \eta)$ is a random variable uniformly distributed between 0 and t_{max}; $\mathcal{U}(0, t_{max}; \eta)$ represents a uniform distribution between 0 and t_{max} and η is the parameter that indexes the realization. If we indicate with t_k^η the delay for the kth shot in the ηth synthetic experiment, we can write the crosstalk matrix as

$$W_{kl} = \sum_\eta \exp^{i\omega[t_l^\eta - t_k^\eta]} = M\delta_{kl} + (1 - \delta_{kl}) \sum_\eta \exp^{i\omega[t_l^\eta - t_k^\eta]} \ . \tag{14}$$

Equation (14) shows that the crosstalk depends on the relative delay difference between different shots. The delay difference changes the spatial location of the artefacts in the image for different realizations of random delays. On the other hand, the correct structural image is always obtained at the correct location. Since the delays are random independent variables, the location of the artifacts will be a random variable as well. The random superposition of the artefacts in space and the null DC component of the wavelet of the recorded signal partially stack out the crosstalk noise. The subsequent stack over different random delay realizations further improves the signal-to-noise ratio, since the positions of the reflectors do not depend on the encoding delays and their contribution will always stack constructively (Romero *et al.* 2000).

Figure 5 shows the evolution of the crosstalk matrix in equation (14), as more synthetic experiments are imaged and stacked and highlights the increasing signal-to-noise ratio described above. The main diagonal is a perfect spike and represents the image we would have obtained by migrating each shot separately. The off-diagonal terms are coupling coefficients between different experiments and are related to

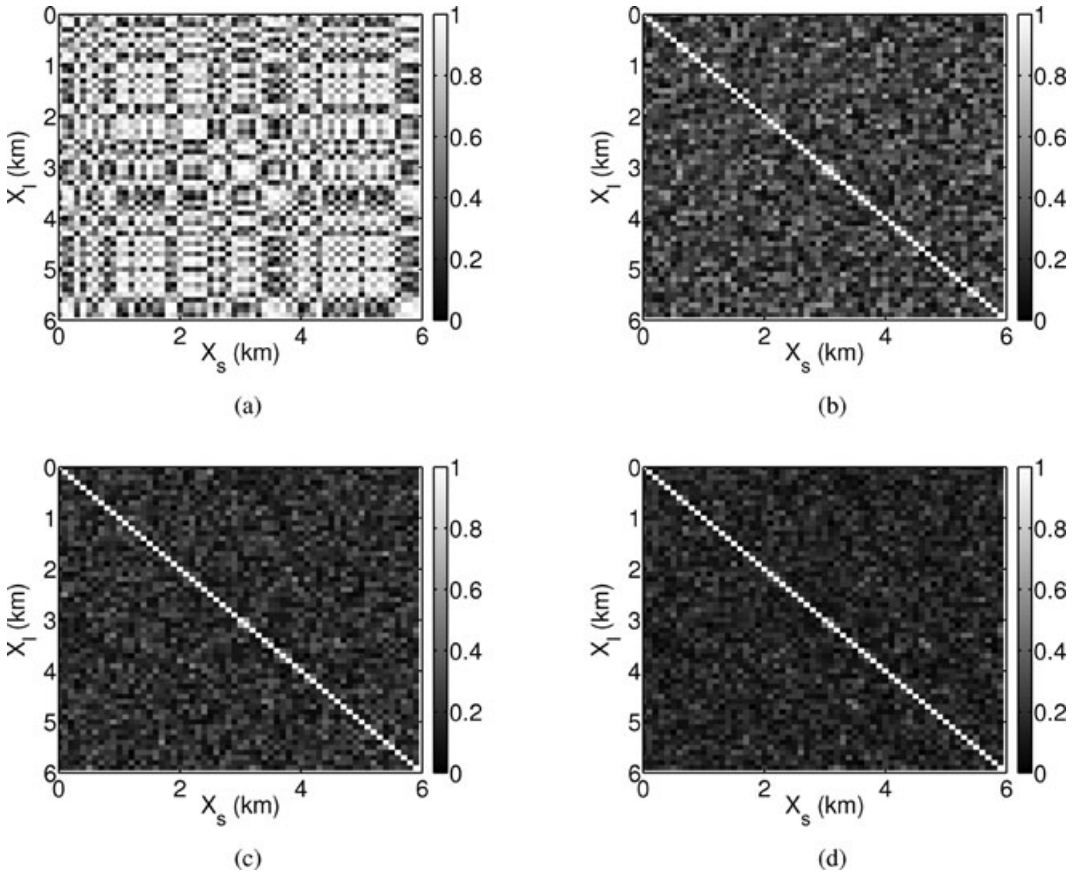


Figure 5 Randon shot-encoding migration crosstalk matrix versus number of synthetic experiments: (a) 2, (b) 10, (c) 20 and (d) 30. The more random-delay realization we consider, the better we approximate the artifact random process. Since the artifacts are zero mean and the stack of a number of experiments is an estimate of the expected value of the process, we are able to remove the crosstalk noise by stacking the images obtained from different random-delay encodings.

crosstalk artefacts. Stacking the images obtained with different realizations of random delays, we decrease the energy of the off-diagonal terms and, consequently, the signal-to-noise ratio increases as the square root of the number of random delay realizations (Romero *et al.* 2000). The image obtained by random shot-encoding approaches the shot-profile migration result as $M \to \infty$.

2.3 Mixed shot-encoding migration

The observations in the previous sections lead to the cartoon in Fig. 2. In the space defined by crosstalk and spatial bandwidth, we can recognize plane-wave migration as one extremum (low crosstalk and low bandwidth) and random shot-encoding as the other extremum (high crosstalk as well as high spatial bandwidth). The cartoon corresponds to a fixed computational cost. We assume a constant computational cost in order to consistently compare the different approaches. We can imagine moving in the space described by crosstalk and spatial bandwidth by combining the previously presented encodings. Our new approach aims to simultaneously reduce the crosstalk and increase spatial bandwidth as we move toward the centre of the crosstalk-bandwidth plane. Of course, the ideal goal is to move towards the upper-right corner (high bandwidth and low crosstalk) and the combination of linear and random shot-encoding is a proxy for this result.

The combination of linear and random shot-encoding involves dithering the plane waves with a random perturbation (Fig. 3c). The expected result is the reduction of crosstalk (because of the side lobes that characterize the crosstalk term for linear shot-encoding) and an increase in spatial bandwidth (given the spikiness of the crosstalk term for random shot-encoding). In Fig. 6, we show the crosstalk matrix for the new

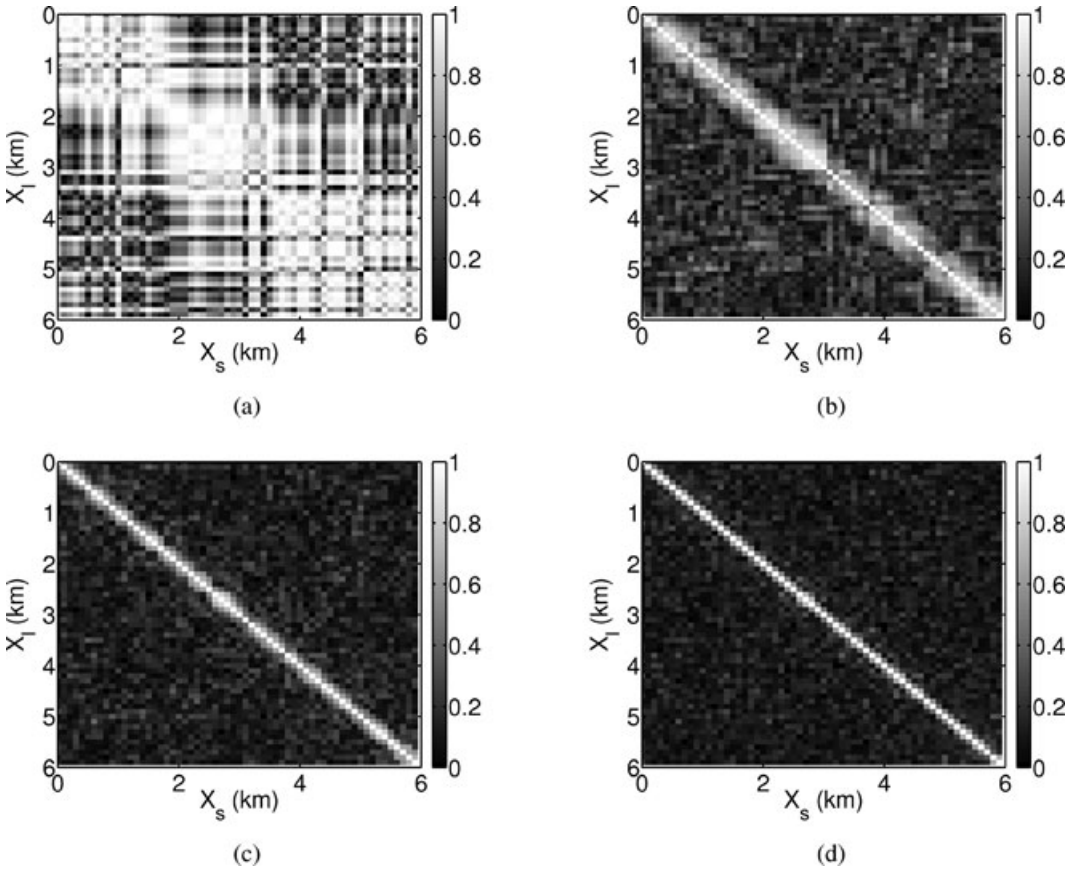


Figure 6 Mixed shot-encoding migration crosstalk matrix versus number of experiments: (a) 2, (b) 10, (c) 20 and (d) 30. Combining linear and random shot-encoding migration, we obtain a crosstalk matrix characterized by a hybrid behavior. In the panels, we observe the linear shot-encoding migration convergence footprint and the random fluctuations due to the wavefront dithering. The dithering is particularly effective in sharpening the main diagonal of the crosstalk matrix.

mixed shot-encoding scheme:

$$W_{kl} = \sum_{\eta} \exp^{i\omega[\mathbf{p}_\eta \cdot (\mathbf{x}_l - \mathbf{x}_k) + (t_l^\eta - t_k^\eta)]} = M\delta_{kl} + (1 - \delta_{kl}) \sum_{\eta} \exp^{i\omega[\mathbf{p}_\eta \Delta \mathbf{x}_{kl} + \Delta t_{kl}^\eta]} \; . \tag{15}$$

We can observe the behaviour in-between linear and random shot-encoding. The crosstalk term partially preserves the characteristic trend of linear shot-encoding with respect to the side lobes, while the dithering destroys the coherency of the side lobes and allows for a spikier main lobe.

Restricting our attention to a single column (row) of the panels in Figs 4–6, we can better appreciate the behaviour with respect to spatial bandwidth and artefacts of linear, random and mixed shot-encoding migration, respectively. Figure 7(a) shows the absolute value of a column (row) of the crosstalk term in the case of linear shot-encoding and 50 plane waves. It is important to note the main lobe and decaying side lobes. Intuitively, we can think of the width of the main lobe as an indicator of the achieved spatial bandwidth, since it describes the coupling between neighbouring shots. The amplitude of the side lobes determines the strength of the artefacts in the image. In this case, we expect a loss in spatial resolution but small artefacts in the final image. We verify these expectations in the result section. For random shot-encoding (Fig. 7b), we observe a spike at $\mathbf{x}_n - \mathbf{x}_m = 0$, when the source and receiver wavefields belong to the same shot, over a random noise floor, which represents the interference between different shots. The spike indicates that we are not trading off the bandwidth of the image; the nonzero terms for $\mathbf{x}_n \neq \mathbf{x}_m$ determine the artefacts. Mixed shot-encoding (Fig. 7c presents a behavior in between linear and random shot-encoding. The spike for the cross-correlation of the wavefields belonging to the same shots ($\mathbf{x}_n - \mathbf{x}_m = 0$) is produced by the dithering, while the linear trend reduces the off-diagonal terms of the crosstalk matrices.

2.4 Crosstalk matrix and approximation to the identity

The effectiveness of the encoding is directly related to the behaviour of the crosstalk matrix. In order to be completely free from artefacts, the sequence of crosstalk matrices must tend to the identity. The encoding problem can then be rephrased in terms of approximation to the identity. In this section, we analyse in greater detail why mixed shot-encoding is more effective in imaging in complex velocity models.

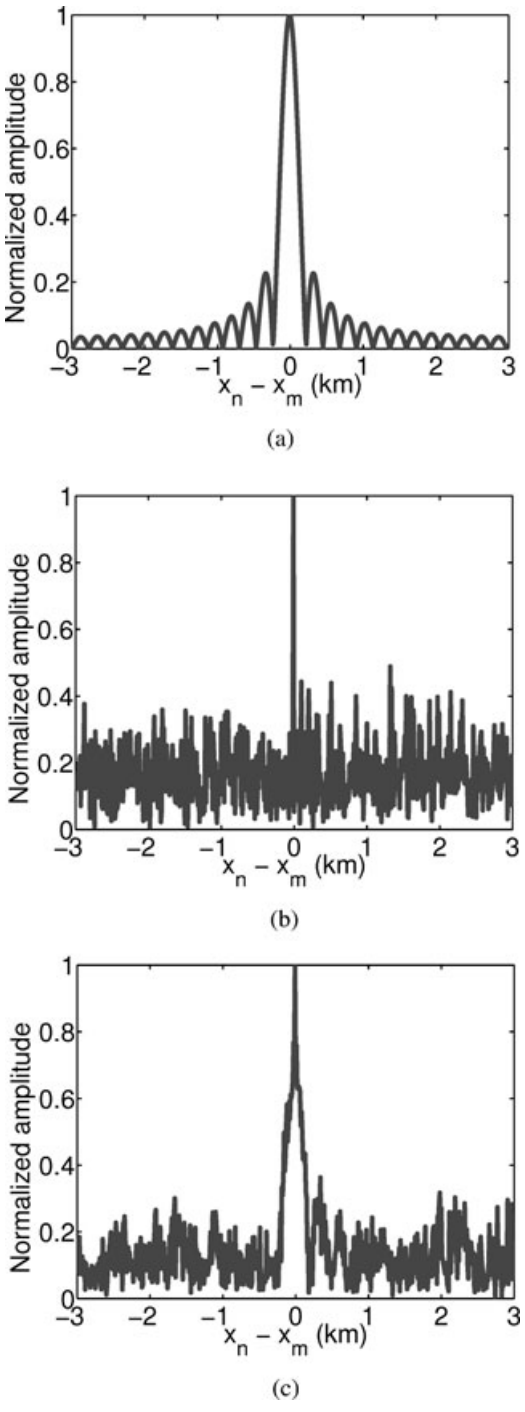


Figure 7 Slices of the crosstalk panel for 50 synthetic experiments: (a) linear, (b) random and (c) mixed shot-encoding migration. They represent the coupling of the wavefields of different shots as a function of the distance between the shots.

The crosstalk term W_{kl} for the three encodings presented in the previous sections is

$$W_{kl}^{L} = \sum_{\eta} \exp^{i\omega \mathrm{p}_{\eta}\cdot(\mathbf{x}_l - \mathbf{x}_k)} , \tag{16}$$

$$W_{kl}^{R} = \sum_{\eta} \exp^{i\omega [t_l^{\eta} - t_k^{\eta}]} , \tag{17}$$

$$W_{kl}^{M} = \sum_{\eta} \exp^{i\omega \left[\mathrm{p}_{\eta}\cdot(\mathbf{x}_l - \mathbf{x}_k) + (t_l^{\eta} - t_k^{\eta})\right]} , \tag{18}$$

for linear, random, and mixed shot-encoding, respectively. In the case of linear and random shot-encoding, equations (16) and (17) actually approximate the identity but from very different points of view. In the first case, the completeness of the Fourier basis functions is invoked; in the second case, the non-correlation of delays in the data and artefacts in the final image yields the result. W_{kl}^{L} converges slowly and smoothly toward the identity operator but does not introduce strong artefacts; in contrast, W_{kl}^{R} converges toward the identity matrix by attenuating the random off-diagonal terms. The off-diagonal terms contribute strong crosstalk, which is iteratively reduced by stacking different synthetic experiments obtained from different random delay realizations.

The crosstalk matrix for mixed shot-encoding in equation (18) can be rewritten as follows:

$$W_{kl}^{M} = \sum_{\eta} \exp^{i\omega \left[\mathrm{p}_{\eta}\Delta\mathbf{x}_{kl} + \Delta t_{kl}^{\eta}\right]}, \tag{19}$$

where $\Delta\mathbf{x}_{kl} = \mathbf{x}_l - \mathbf{x}_k$ represents the distance vector between shot locations and $\Delta t_{kl} = t_l^{\eta} - t_k^{\eta}$ is the time dithering difference. Separating the terms for $k = l$ and collecting $\Delta\mathbf{x}_{kl}$ in the exponent yields

$$W_{kl}^{M} = M\delta_{kl} + (1 - \delta_{kl}) \sum_{\eta} \exp^{i\omega \left[\left(\mathrm{p}_{\eta} + \frac{\Delta t_{kl}^{\eta}}{\Delta\mathbf{x}_{kl}}\right)\Delta\mathbf{x}_{kl}\right]} . \tag{20}$$

The ratio $\frac{\Delta t_{kl}^{\eta}}{\Delta\mathbf{x}_{kl}}$ has the dimensions of a ray parameter and can be viewed as a perturbation of the ray parameter $\mathbf{p}_{\eta}$. Note that the perturbation varies spatially since it depends on $\Delta\mathbf{x}_{kl}$; the non-stationary nature of the ratio $\frac{\Delta t_{kl}^{\eta}}{\Delta\mathbf{x}_{kl}}$ allows us to gain spatial resolution with respect to standard plane-wave migration, since a greater number of 'equivalent' spatial components $p_{\eta}^{eq} = \mathbf{p}_{\eta} + \frac{\Delta t_{kl}^{\eta}}{\Delta\mathbf{x}_{kl}}$ is imaged; however, it also introduces a disturbance in the convergence of the crosstalk matrix toward the identity operator, i.e., random-like artefacts in the final image.

Let us consider two limiting cases. If $\Delta\mathbf{x}_{kl}$ is small/large, i.e., if we are close to one particular shot location, we have

$$\mathbf{p}_{\eta}^{eq} = \mathbf{p}_{\eta} + \frac{\Delta t_{kl}^{\eta}}{\Delta\mathbf{x}_{kl}} \longrightarrow \frac{\Delta t_{kl}^{\eta}}{\Delta\mathbf{x}_{kl}}; \tag{21}$$

on the contrary, if $\Delta\mathbf{x}_{kl}$ is 'large', i.e., if we are considering the mutual influence of two distant shots, we have

$$\mathbf{p}_{\eta}^{eq} = \mathbf{p}_{\eta} + \frac{\Delta t_{kl}^{\eta}}{\Delta\mathbf{x}_{kl}} \longrightarrow \frac{\sin(\alpha\eta)}{v}. \tag{22}$$

Mixed shot-encoding behaves like random shot-encoding (see equation 21) when we consider neighbouring shots and resembles linear shot-encoding when we analyse the effects on a particular shot from more distant ones (see equation 22). This different behaviour explains the increase in the spatial resolution (compared to linear shot-encoding) and the decrease in crosstalk (compared to random shot-encoding) that mixed shot-encoding is able to achieve.

The analysis of the distribution of the resulting random variable $\frac{\Delta t_{kl}^{\eta}}{\Delta\mathbf{x}_{kl}}$ is not straightforward; even though we can intuitively understand $\frac{\Delta t_{kl}^{\eta}}{\Delta\mathbf{x}_{kl}}$ as a random perturbation of a fixed ray parameter $\mathbf{p}_{\eta}$, this perturbation is now spatially-varying along the shot positions because of the term $\Delta\mathbf{x}_{kl}$. This is counterintuitive since we usually associate a ray parameter with a planar wavefront rather than with one that is dithered and not well-defined.

An alternative way of looking at this is to imagine simultaneously migrating a bundle of plane-waves that are randomly chosen in the neighbourhood of a given $\mathbf{p}_{\eta}$. Actually, mixed shot-encoding images more plane-wave components than linear shot-encoding; indeed, it images all the plane-wave components available in the data but with uneven relative amplitudes.

2.5 Example of a point scatterer in a constant background

We illustrate the features highlighted in the previous sections with a simple exercise that images a point scatterer in a constant velocity background. We compare the results obtained by stacking 10 images constructed with linear, random and mixed shot-encoding (Fig. 8). In all three cases, the maximum delay applied to wavefields is the same and is equal to 1 s. For imaging algorithms implemented in the time domain, like reverse-time migration, the fixed maximum delay ensures that all migrations have the same cost, regardless of the encoding type.

Notice the lower focus of the image obtained by linear shot-encoding (Fig. 8a). The point is spread in the horizontal

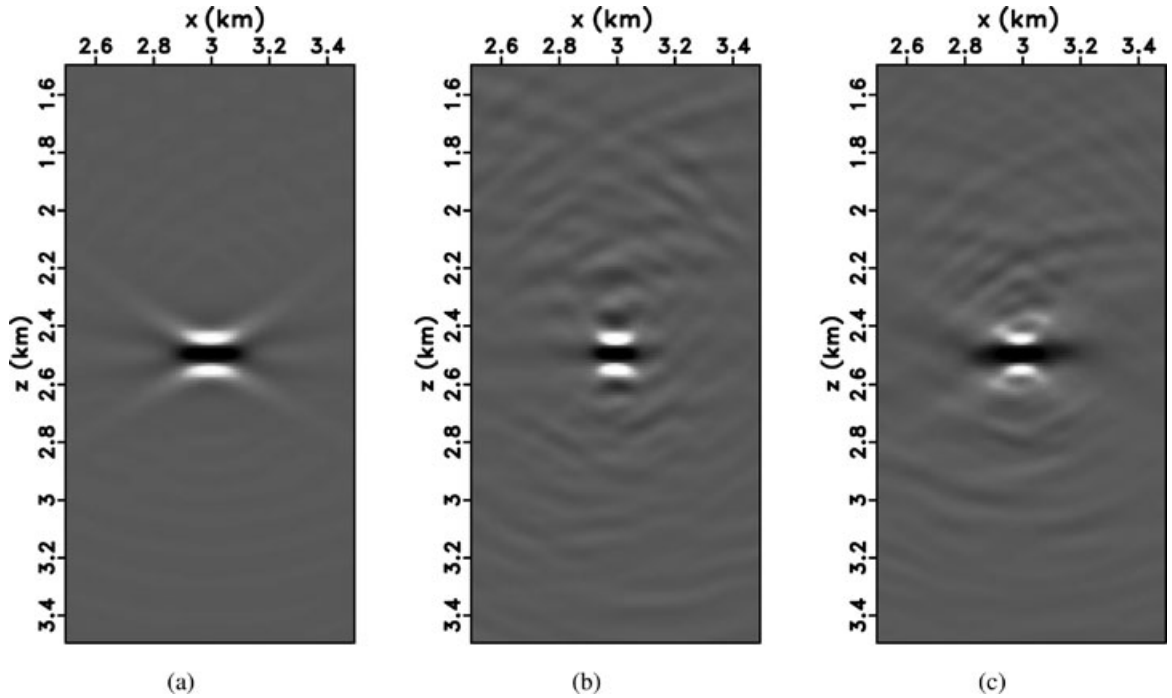


Figure 8 Point scatterer in a constant medium: (a) linear, (b) random and (c) mixed shot-encoding migration. Observe the horizontal spreading in linear shot-encoding migration; the limitation in spatial components reduces the spatial bandwidth of the image. Random shot-encoding migration produces a sharper image but creates artifacts; mixed shot-encoding migration provides more spatial detail and limits the crosstalk in space compared to linear and random shot-encoding migration, respectively.

direction because we have not considered plane waves with high values of η in the imaging process, i.e., with a high ray parameter **p**. On the other hand, the image is clean because the crosstalk decreases quickly with the distance $(\mathbf{x}_k - \mathbf{x}_l)$. random shot-encoding (Fig. 8b) represents the other extremum in the trade-off between crosstalk and spatial bandwidth. In this case, a wider range of the spatial components is imaged but crosstalk noise is present in the image as well. The synthetic experiments contain more events than the single shot-profile data and then for an encoded image the crosstalk is maximized. The stack of the different experiments is effective for this simple model but the result rapidly worsens with increasing complexity of the subsurface. Figure 8(c) shows the image obtained by mixed shot-encoding migration. We can observe a spatial resolution that is closer to random shot-encoding migration but has fewer artefacts over a smaller spatial extent.

3 SIGSBEE EXAMPLE

In the previous section, we have analyzed the mixed shot-encoding algorithm in the case of a point scatterer in a homogeneous velocity model. We point out the reduction in crosstalk with respect to random shot-encoding, and the increase in spatial bandwidth with regard to linear shot-encoding migration when the range of take-off angles is kept fixed. Here, we verify these results in a more realistic case.

The crosstalk in the final image is heavily dependent on the complexity of the model. In a complex, heterogeneous velocity model, plane waves are distorted and the phase relations that define W_{kl} break down as soon as inhomogeneities are encountered. Nonetheless, random shot-encoding may be more robust in regard to this problem since there is no phase coherency to be preserved.

Let us consider the complex Sigsbee model distributed by SMAART JV (Paffenholz *et al.* 2002). First, we migrate the entire survey and obtain the benchmarck image by imaging all 500 shots. The result is shown in Fig. 9(a). The velocity model used for migration is the exact one and thus the obtained image represents the optimum migration result.

Undersampling the shot dimension by a factor of 5, we obtain the image in Fig. 9(b). Despite the correctness of the velocity model, we observe residual migration smiles in poorly illuminated areas of the image ($z = 5.0$ km below the salt body and in the deepest part of the model at $z = 8.0$ km) or in

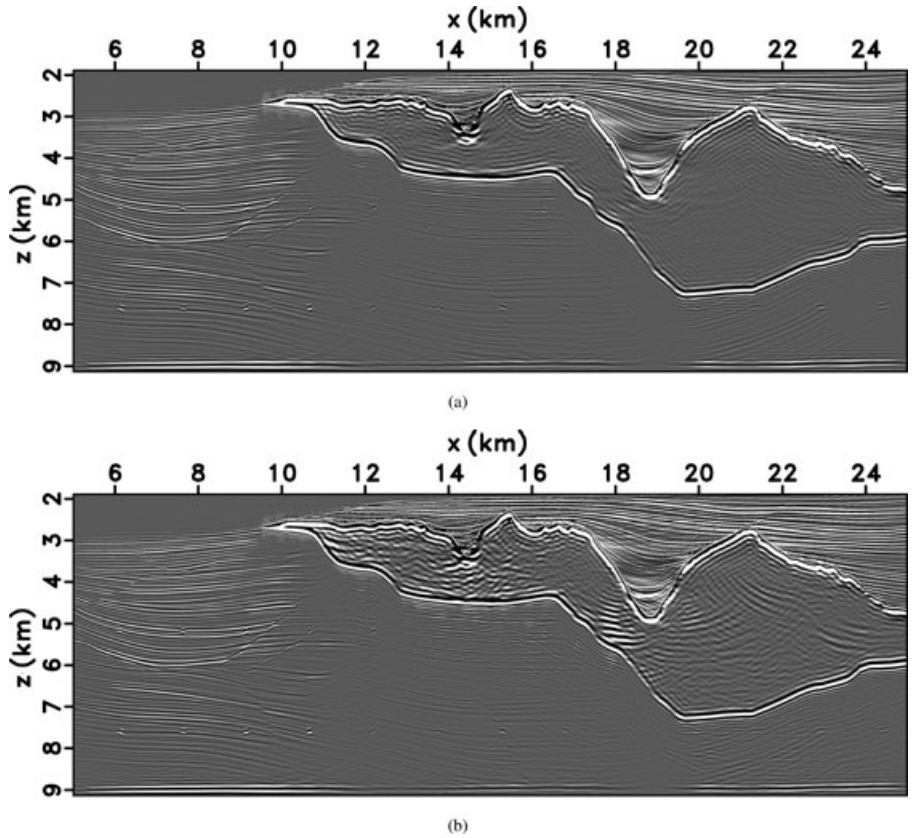


Figure 9 Shot-profile migration of the Sigsbee data set; (a) stack of all 500 shot-record migrations, (b) stack of 100 evenly-spaced shots. Observe the residual migration smiles below the salt body.

particularly complex areas, like the salt canyon at ($x = 19.0$ km, $z = 4.0$ km). This first result shows that the shot domain is sensitive to shot sampling and spacing; moreover, the sensitivity depends on the local illumination. In the following, we compare the results obtained with linear, random and mixed shot-encoding migration for different numbers of synthetic shot-gathers and different take-off angle ranges. The goal is to show that we can reduce the sensitivity to the maximum value of the ray-parameter and we can control the crosstalk noise in the final image.

Zhang *et al.* (2005) obtained an expression for computing the number of plane-wave components needed to obtain an image equivalent to shot-profile migration, given the maximum temporal frequency in the data, the survey aperture and the range of take-off angles at the surface. Considering the take-off angle in the range from -30 to 30 degrees, a maximum frequency of 10 Hz and an aperture equal to the survey length, the expression in Zhang *et al.* (2005) returns a value of $N_p = 150$ plane-wave components. We migrated the data using the specified parameters and obtained the image in Fig. 10(a). Comparing this result with Fig. 9(a), we observe an excellent agreement between the two images. Linear shot-encoding migration can be considered more than 3 times cheaper than shot-profile migration in this example.

If we consider the same number of synthetic shot-gathers for random and mixed shot-encoding migration, we obtain the results in Fig. 10(b,c), respectively. Linear shot-encoding migration outperforms random and mixed shot-encoding when we correctly sample the take-off angle and all the dips in the image are illuminated. For random shot-encoding migration, the delay applied to each shot is a random variable uniformly distributed between 0 and the maximum delay 11 s. The dithering applied to the planar wavefront is 5% of the maximum delay. For synthetizing a plane wave with a take-off angle of 30 degrees, the maximum delay is 11 s and the dithering is about 0.5 s.

In the context of reverse-time migration, the delay we need to apply to synthesize plane-wave shot-gathers directly impacts the computational cost of imaging. This is because the wavefields are extrapolated in time and a longer shot-record

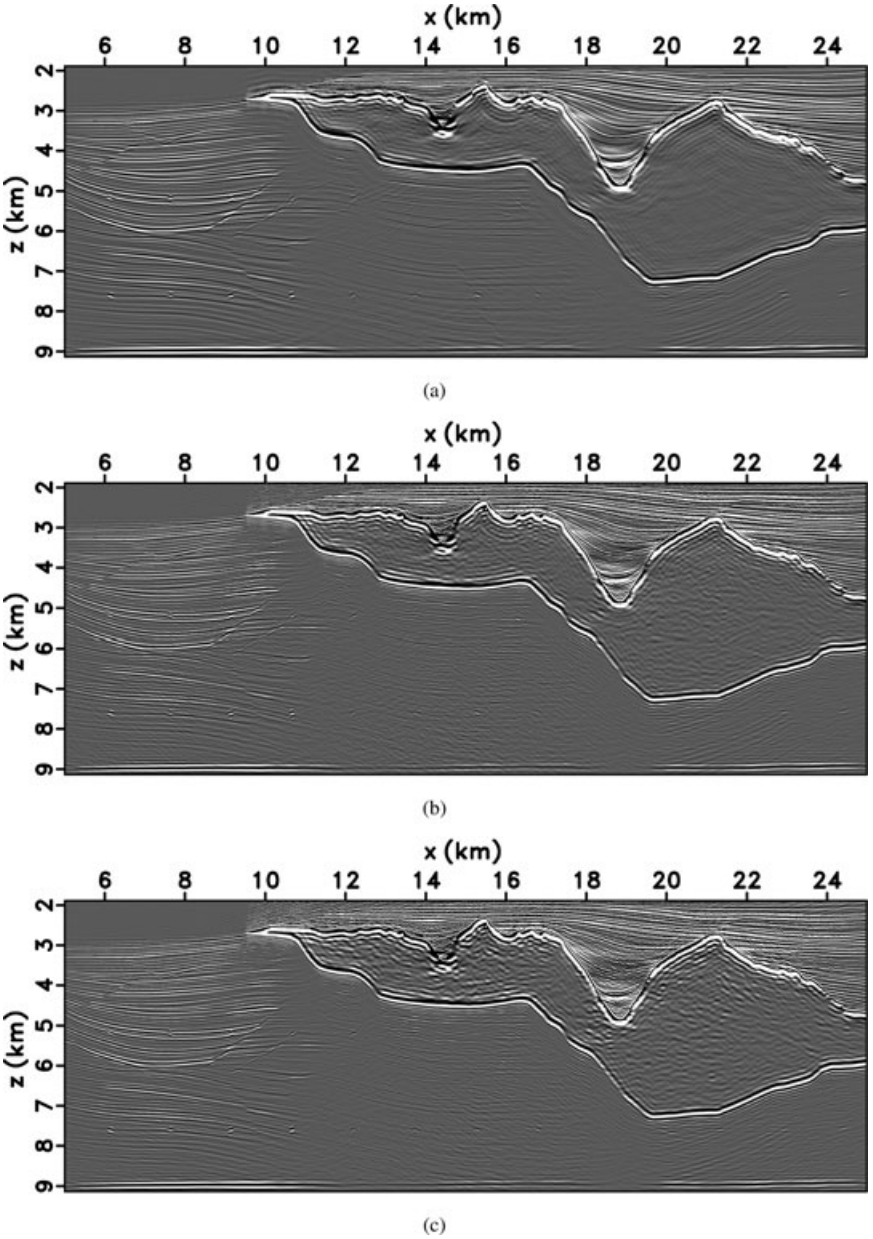


Figure 10 Sigsbee data set migrated using different encoding schemes: (a) linear, (b) random and (c) mixed shot-encoding migration. 150 synthetic experiments were used for each encoding method. The number of experiments is consistent with the expression in Zhang *et al.* (2005). The take-off angle range is from −30 to 30 degrees. The plane-wave dithering used in mixed shot-encoding migration is 5% of the maximum delay in linear shot-encoding migration.

implies a longer extrapolation time and more finite-difference iterations. In order to reduce the computational cost, we are thus interested in reducing the maximum delay or the range of take-off angles considered.

In our experiments, we reduce the range of take-off angles for linear shot-encoding migration. We consider the range from −15 to 15 degrees, which is equivalent to a maximum delay of 4 s. The number of synthesized shot-gathers obtained from the expression in Zhang *et al.* (2005) is $N_p = 53$. In Fig. 11, we show the results obtained from linear, random and mixed shot-encoding migration. Limiting the range of take-off angles in plane-wave migration, we lose spatial detail (the steeply dipping events at about $x = 10.0$ km below the salt nose and point diffractors are not imaged correctly or not

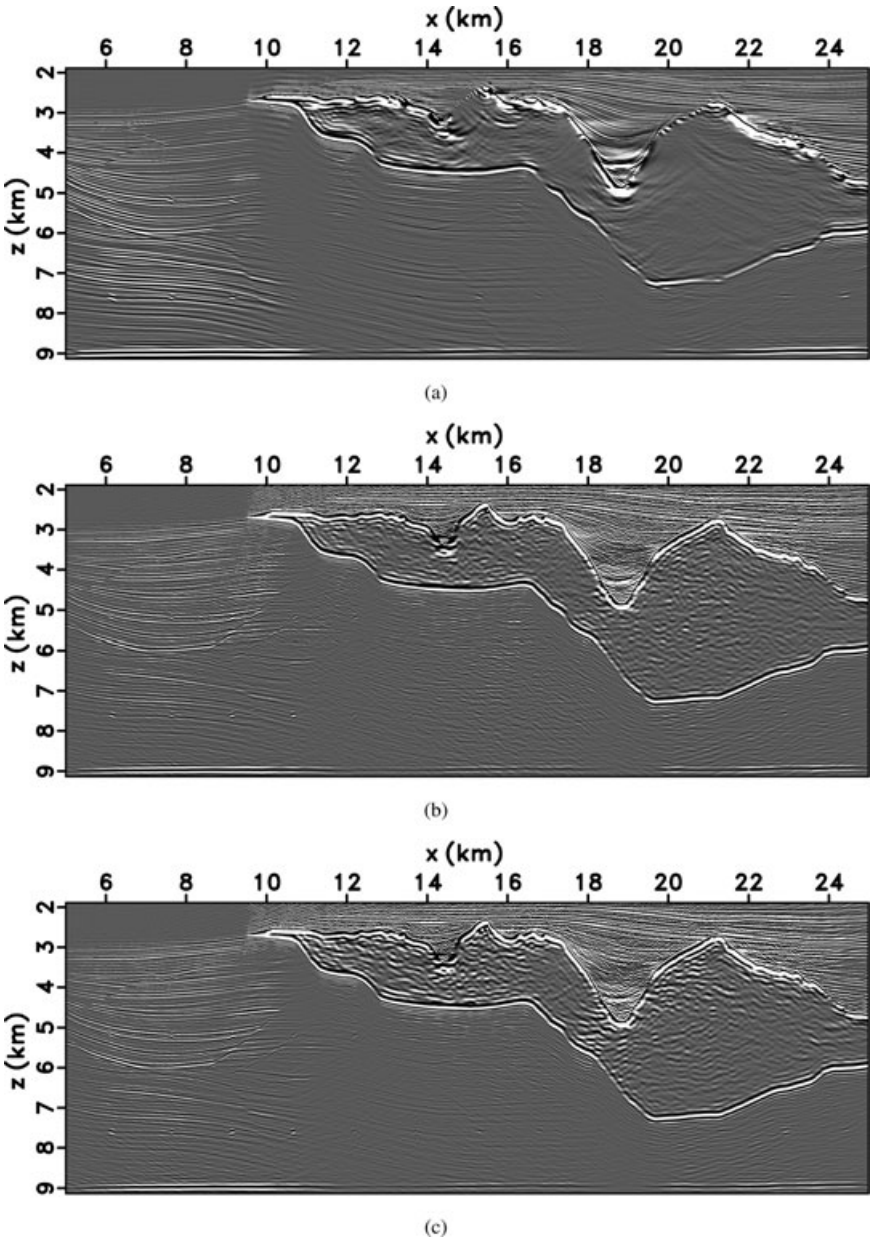


Figure 11 Sigsbee data set migrated using different encoding schemes: (a) linear, (b) random and (c) mixed shot-encoding migration. The take-off angle range is from −15 to 15 degrees. The plane-wave dithering used in mixed shot-encoding migration is 5% of the maximum delay in linear shot-encoding. 53 synthetic experiments were used for each encoding method. The number of experiments is consistent with the expression in Zhang *et al.* (2005).

imaged at all). Random and mixed shot-encoding migrations return a more complete image in terms of spatial resolution but they introduce crosstalk artefacts. Mixed shot-encoding is more effective than random shot-encoding in controlling the migration noise due to crosstalk. The dithering applied to the planar wavefront is again 5% of the maximum delay.

As we discussed in the previous sections, mixed shot-encoding migration is a hybrid scheme that combines linear and random shot-encoding. By increasing the applied dithering, we can move from linear to random encoding with continuity. In Fig. 12, we compare linear and mixed encoding using the same number of synthetic shots used in the previous case

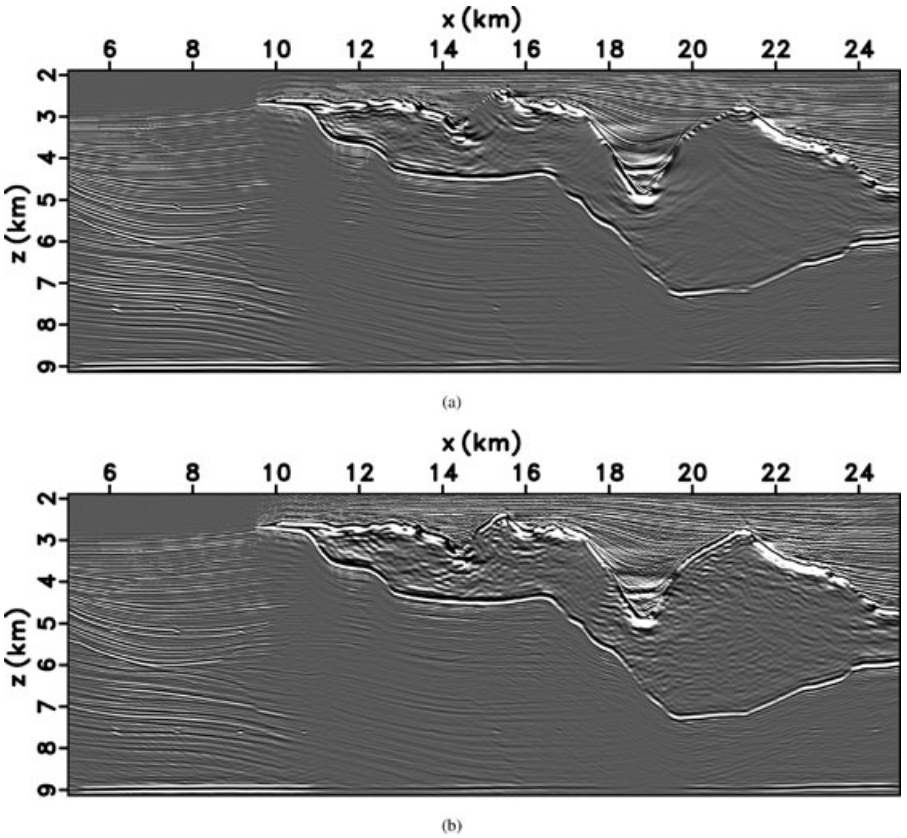


Figure 12 13 Sigsbee data set migrated using (a) linear and (b) mixed shot-encoding migration. The take-off angle range is from −15 to 15 degrees. The plane-wave dithering used in mixed shot-encoding migration is 0.8% of the maximum delay in linear shot-encoding migration. 53 synthetic experiments have been used for each encoding method. The number of experiments is consistent with the expression in Zhang *et al.* (2005).

and the same range of take-off angles for linear shot-encoding but we decrease the dithering for mixed shot-encoding migration to 0.8%. For facilitating the analysis, Fig. 12(a) shows the same result as Fig. 11(a). Comparing Figs 12(a) and 12(b), we observe the decrease in crosstalk noise while the spatial details are preserved (faults at $x = 10.0$ km below the nose of the salt). Especially below the salt body ($z = 5.0$ km), the stratigraphy is better recovered, the reflectors are imaged right below the nose of the salt and the faults and point scatterer are recovered.

Reducing the number of synthetic experiments also decreases the effectiveness of stacking for attenuating the artefacts due to the dithering of the planar wavefront. We then increase the number of synthetic shot-gathers (106 instead of 53, in the previous example) and process them using linear and mixed shot-encoding migration. We keep fixed the take-off angle range (from −15 to 15 degrees) and the dithering (0.8% of the maximum plane-wave delay). In the framework of reverse-time migration, this solution allows for shorter shot-gathers without reducing the steep dip information in the final image. Figure 13 shows how the maximum ray parameter in linear shot-encoding migration limits the spatial detail we can actually image. Oversampling the **p**-axis does not increase the spatial resolution of the final image. On the contrary, by increasing the number of dithered plane waves we can effectively attenuate the crosstalk noise without affecting the steeply dipping event information. The result in Fig. 13(b) has a computational cost about 5 times smaller than the conventional shot-profile image.

It is interesting to look at the effects of the amount of dithering on the quality of the final image. Intuitively, we obtain the linear shot-encoding image by reducing the dithering but the relationship between the amount of perturbation and the increase in the spatial bandwidth of the image cannot easily be evaluated. In Fig. 14(a), we show the standard plane-wave migration image. The range of take-off angles is from −15

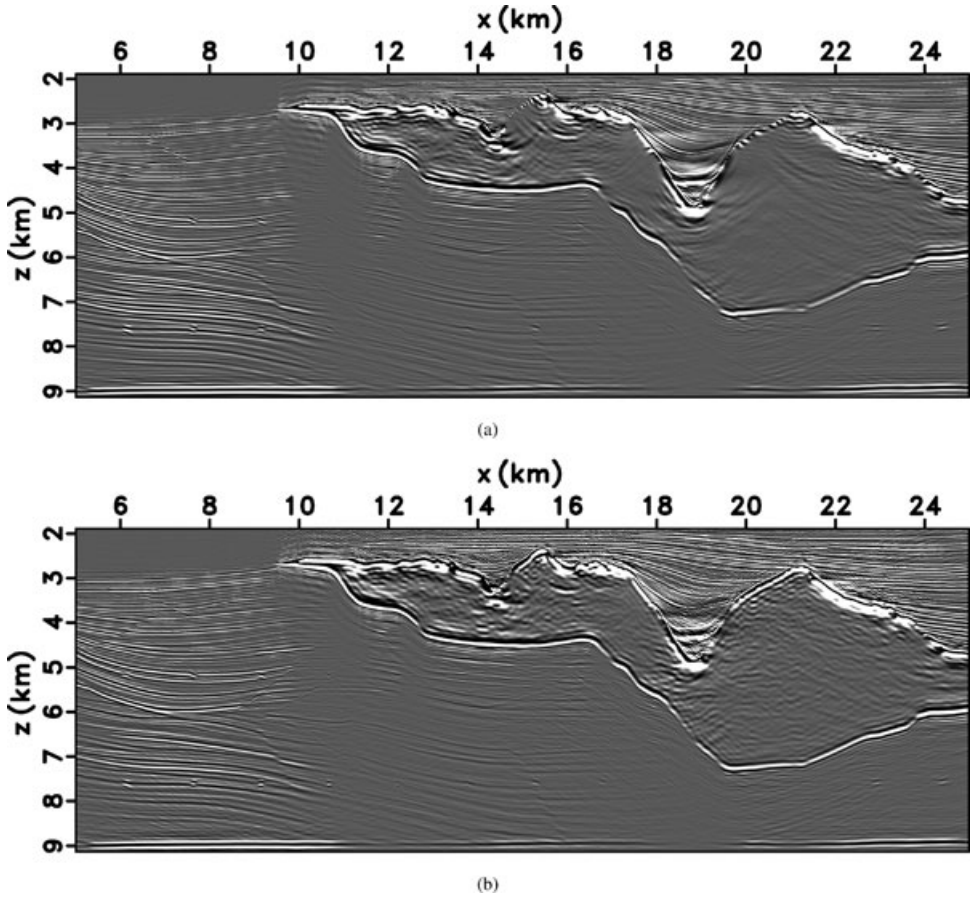


Figure 13 Sigsbee data set migrated using () linear and (b) mixed shot-encoding migration. The take-off angle range is from −15 to 15 degrees. The plane-wave dithering used in mixed shot-encoding migration is 0.8% of the maximum delay in linear shot-encoding migration. 106 synthetic experiments were used for each encoding method. We increased the number of experiments to increase the signal-to-noise ratio in the image without increasing the maximum delay of the synthetic shot-gathers.

to 15 degrees and we are not able to illuminate the steeply dipping faults below the nose of the salt ($x = 10.0$ km), nevertheless the horizontal features in the image are well-imaged. Figure 14(b– e) is obtained using mixed shot-encoding migration with dithering equal to 1%, 5%, 20% and 30%, respectively. Note the considerable increase in spatial detail achieved with respect to plane-wave migration. The faults in the image are now interpretable and the point scatterers are better reconstructed. Nonetheless, below the salt body, the quality of the image decreases with increasing dithering. Figure 14(e) is analogous to the image obtained using random shot-encoding migration in Fig. 14(f) where the illumination is poor.

It is difficult to quantify the optimum dithering because of the model-dependence of the problem. Given a data set, we could estimate it *a posteriori* by considering different image-quality indicators (spatial spectrum, image entropy, etc.) but this strategy would reduce the cost-effectiveness of mixed shot-encoding migration.

We obtain common-image gathers for linear and mixed shot-encoding migration for both the correct and an incorrect velocity model. The common-image gathers were extracted at different locations in order to analyse the effect of the model heterogeneity. Figure 15(a) shows the common-image gather at $x = 8.68$ km for linear shot-encoding migration and Fig. 15(b) shows the same gather for mixed shot-encoding migration. In the sediment zone ($x = 8.68$ km), the results are comparable: we can identify the same events and, in fact, the plane-wave dithering supplies extra illumination. The events are more continuous over a larger range of experiments than in linear shot-encoding. We observe a reduction of coherent migration artefacts in the salt area (compare Figs 16a and 16b) and an increase of incoherent noise due to the plane-wave dithering. Actually, while the gathers for the two encoding are

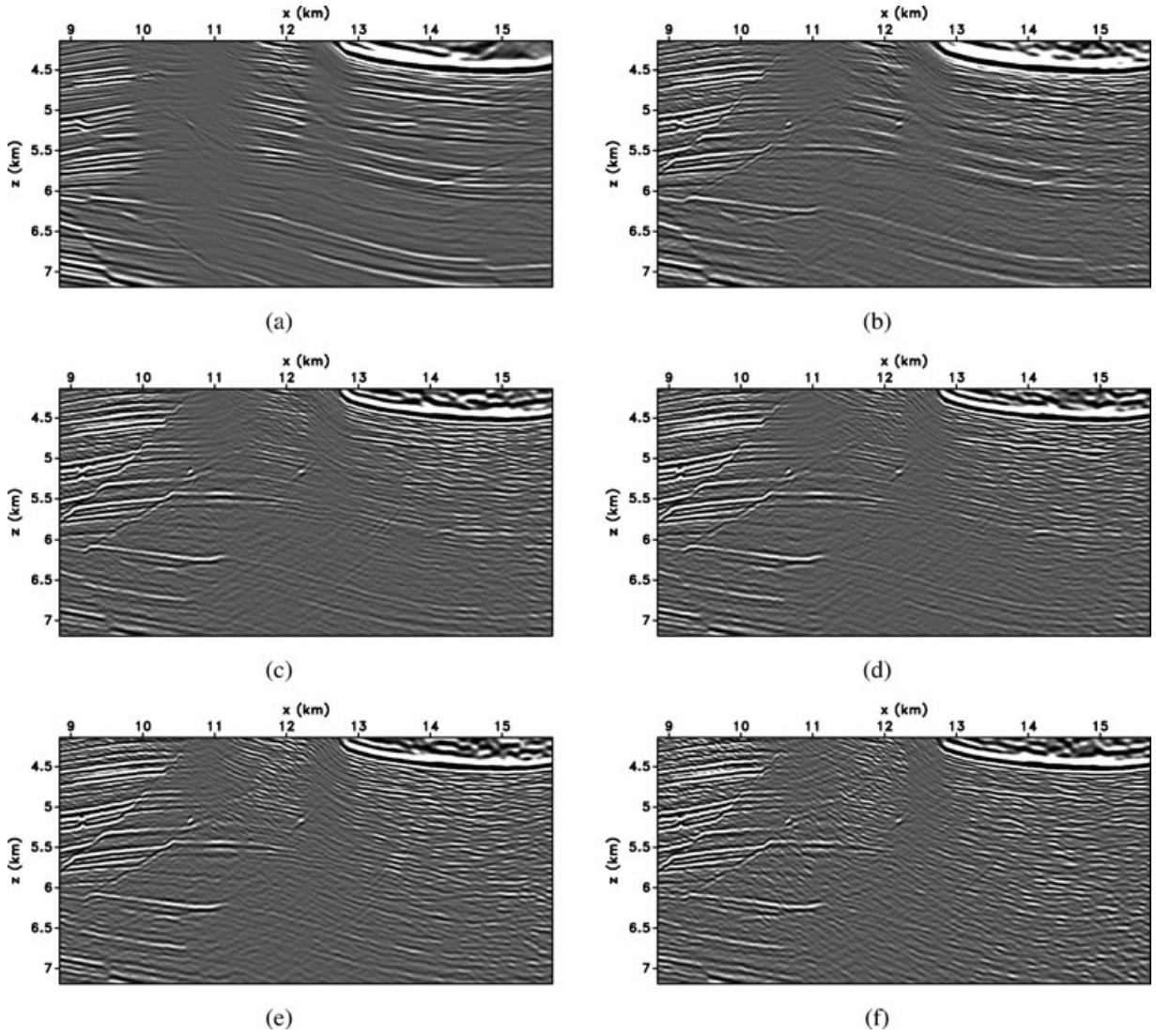


Figure 14 Effect of the amount of dithering on a poorly illuminated area of the image. The images refer to linear shot-encoding migration, 1%, 5%, 20%, 30% dithering and randon shot-encoding migration, respectively. Increasing the dithering we move from a result that resembles plane-wave migration to a result similar to random shot-encoding migration, especially below the salt body.

quite comparable below the salt, mixed shot-encoding introduces strong crosstalk above the salt body. The events visible in the stacked section are due to the destructive interference of the crosstalk in the prestack panels.

If the velocity model is incorrect, the events in the common-image gathers are not flat (Figs 17 and 18). The velocity model for this example is uniformly 5% slower than the correct one. Because the dithering applied to the reference planar wavefront is small (0.8% of the maximum delay, in these examples), we expect mixed shot-encoding to produce gathers similar to linear shot-encoding. We extract gathers at the same horizontal locations ($x = 8.68$ km and $x = 13.0$ km). The two encodings do show similar behaviour in the common-image gather domain. Nevertheless, because of the constraint on the maximum delay, very little moveout is observed. For mixed shot-encoding, the gathers in the sediment area (Fig. 17b) are more easily interpretable than in the salt area (Fig. 18b). The dithering reduces coherent migration artefacts due to the limited range of plane-wave components but it also introduces random noise due to the crosstalk artefacts.

4 DISCUSSION

The reduction of the computational cost using synthetic shot-gathers and encoded migration is constrained by two factors:

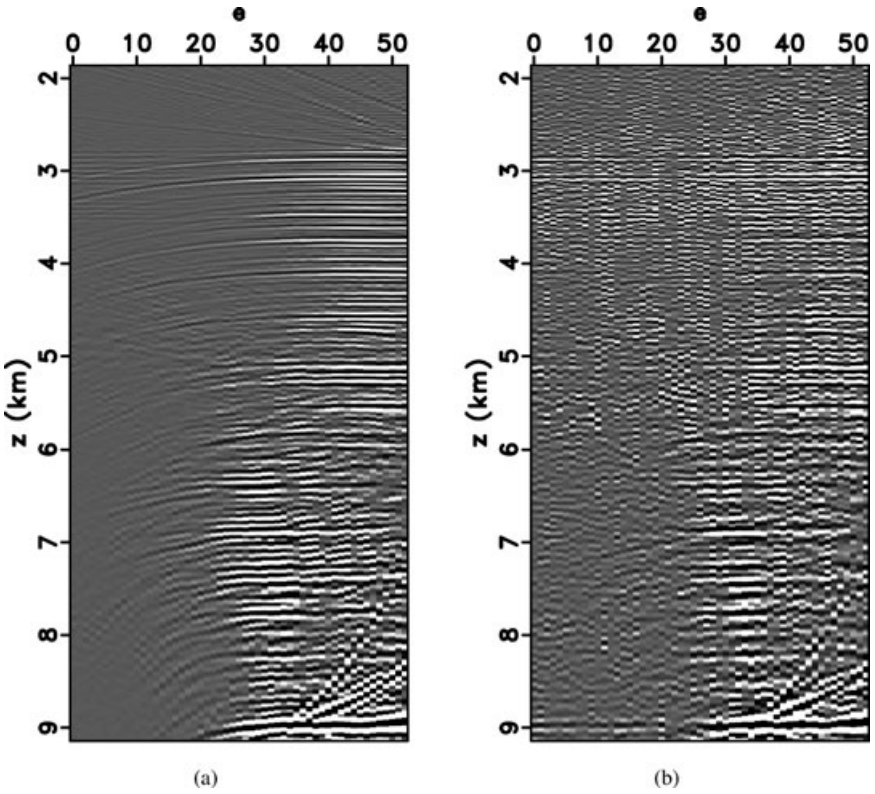


Figure 15 Common-image gather in the sediment area of the Sigsbee model ($x = 8.68$ km) obtained using (a) linear and (b) mixed shot-encoding migration with the correct velocity model. The label e on the horizontal axis stands for 'experiments'; for linear shot-encoding migration, this axis represents the take-off angle of the source plane waves. The take-off angle range is from −15 to 15 degrees.

first, the spatial bandwidth that we want to recover in the migrated image; second, the crosstalk noise that is introduced in the final result.

The examples presented in the previous sections show the robustness of mixed shot-encoding against artefacts produced by crosstalk between different shots. A single point scatterer in a homogeneous velocity medium is imaged with more spatial components compared to linear shot-encoding when the range of take-off angles is limited. Hence, mixed shot-encoding partially spans the domain in between the two extremal strategies represented by linear and random shot-encoding.

Shot-encoding strategies are preferable to shot undersampling. If the shot domain is undersampled, the migration smiles due to the limited aperture of the single experiments do not cancel completely and, especially in poorly illuminated parts of the model, they constitute a strong source of coherent noise, which interferes with the imaged structured (compare Fig. 9a,b). Nonetheless, shot-encoding introduces crosstalk noise due to the interference between source and receiver wavefields from different physical experiments. This crosstalk noise is attenuated stacking several shot-encoding migrations but the impact on the image quality strongly depends on the local illumination.

When a sufficient number of plane-wave components is used and the ray-parameter sampling is correct, the optimality of linear-shot-encoding is evident by comparison with the results obtained with random and mixed shot-encoding migration (Fig. 10b,c). The images appear quite noisy and the reflectors are not well-imaged. For a large number of synthetic experiments, random and mixed shot-encoding supply comparable results in terms of image-quality with respect to linear and shot-profile migration.

The situation changes if the range of take-off angles is limited (for example, from −15 to 15 degrees). This solution becomes attractive in the framework of reverse-time migration, where the maximum take-off angle, i.e., the maximum delay, fixes the computational cost of the imaging step. Again, the number of plane-wave components is computed using the expression in Zhang *et al.* (2005) ($N_p = 53$) and then we correctly sample the take-off angle dimension. As shown in Fig 11, linear shot-encoding migration is sensitive to the maximum take-off angle considered since it limits the

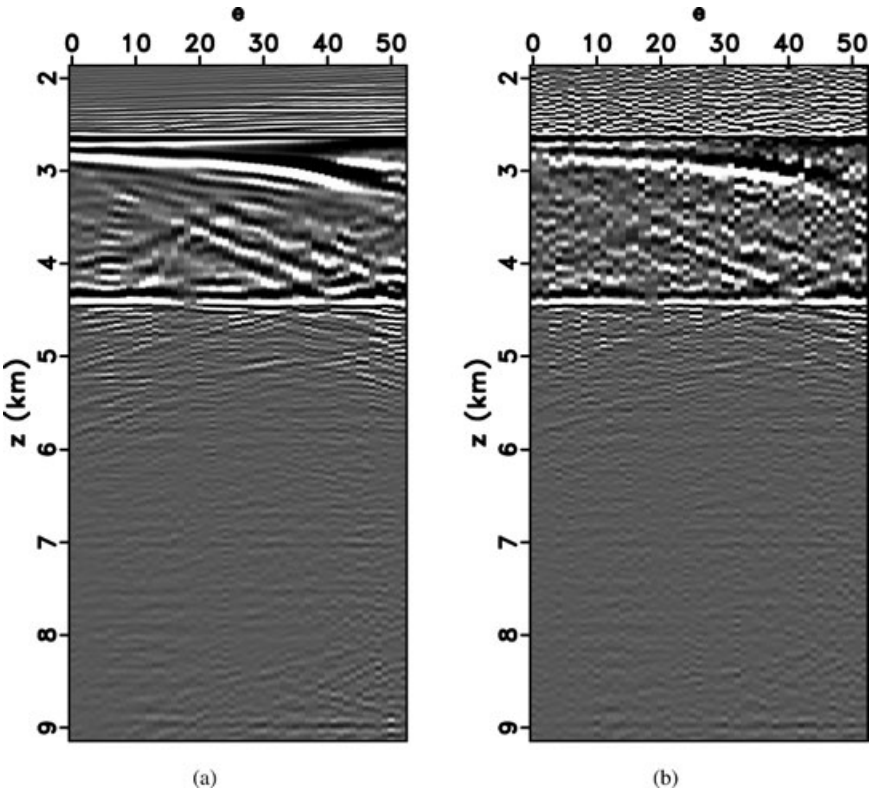


Figure 16 Common-image gather in the salt area ($x = 13.0$ km) obtained using (a) linear and (b) mixed shot-encoding migration with the correct velocity model. The label *e* on the horizontal axis stands for 'experiments'; for linear shot-encoding migration, this axis represents the take-off angle of the source plane waves. The take-off angle range is from −15 to 15 degrees.

spatial wavenumber components that can be imaged. By limiting the range of ray-parameters, steeply dipping events are not correctly or accurately imaged and only nearly horizontal events are clearly imaged (Fig. 11a). On the contrary, random shot-encoding migration is quite insensitive to the maximum delay used for encoding the sources. Using the maximum delay in linear shot-encoding for defining the delay distribution in random shot-encoding, we obtain the image in Fig. 11(b). The spatial bandwidth of the image can be completely imaged but in poorly illuminated areas the crosstalk noise overwhelms the signal. In this case, a greater number of synthetic experiments should be stacked for attenuating the noise, reducing the cost effectiveness of the procedure. Mixed shot-encoding migration (Fig. 11c) shares features of linear and random shot-encoding migration. A better imaging of nearly horizontal events is achieved compared to random shot-encoding and steeply dipping events and faults, which are not visible in Fig. 11(a), are correctly imaged. Residual crosstalk is in the image, especially immediately below the salt body ($z = 5.5$ km), but at greater depths (for example, $z = 7.5$ km) we can pick the same events visible in the linear shot-encoding migration image.

The maximum delay we use in the encoding procedure defines the cost in time-domain migration schemes like reverse-time migration. By constraining the maximum delay, we limit the maximum take-off angle in linear shot-encoding migration. This limitation affects the spatial resolution of the final image, especially in the case of complex velocity models, because not all the wavenumbers are illuminated. Random shot-encoding migration is able to image all the possible wavenumbers of the model but the limited number of experiments hampers the attenuation of the crosstalk noise the imaging scheme produces. Mixed shot-encoding migration represents a compromise between spatial detail in the image (in terms of recovered wavenumbers) and crosstalk. In particular, mixed shot-encoding migration appears to be less sensitive to the range of take-off angles considered because the dithering introduces extra spatial components that are not imaged by standard plane-wave migration. Nonetheless, some noise is present and the reduced number of synthetic experiments do not allow a complete cancellation, especially above the salt body. The simplest solution for increasing the signal-to-noise ratio is to image more synthetic shot gathers. In the framework of reverse-time migration, the length of the shot-gather

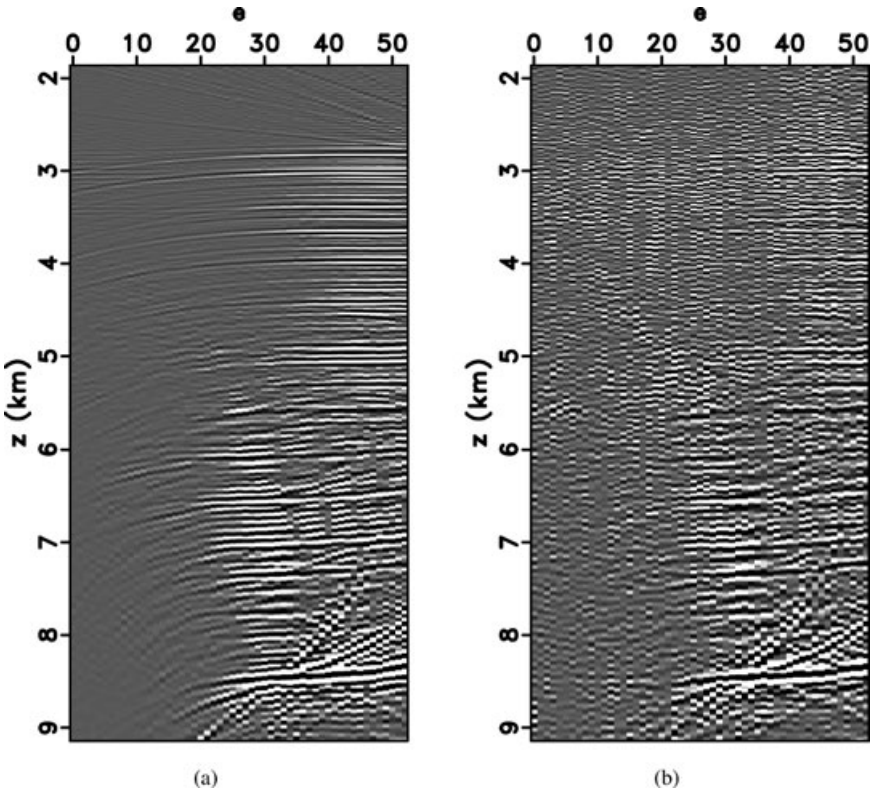


Figure 17 Common-image gather in the sediment part of the Sigsbee model ($x = 8.68$ km) obtained using (a) linear and (b) mixed shot-encoding migration with a 5% slower velocity model. The label *e* on the horizontal axis stands for 'experiments'; for linear shot-encoding migration, this axis represents the take-off angle of the source plane waves. The take-off angle range is from −15 to 15 degrees.

directly affects the total computational cost of the imaging step. As we have already observed, mixed shot-encoding is able to image steeply dipping events and high wavenumber information despite the limitation of the take-off angle range. Mixed shot-encoding migration allows us to constrain the maximum length of the synthetic shot-gathers, to attenuate the crosstalk noise through the number of synthetic experiments considered and preserve the structural information in the image.

From the numerical tests, mixed shot-encoding migration results are more effective than linear shot-encoding migration when a very limited range of take-off angles is used. Mixed shot-encoding migration is also better-behaved than random shot-encoding migration when the crosstalk in the final image is considered and a small number of synthetic shot-gathers is imaged. With respect to undersampling in the shot domain, we reduce the coherent noise due to the incomplete cancellation of migration smiles but we do introduce incoherent noise. Depending on the particular application, mixed shot-encoding may be preferable for fast-picking of common-image point gather locations (Sava and Vasconcelos 2009; Vasconcelos, Sava and Douma 2010) because no coherent artifacts are present in the image and reflectors can be more easily identified, especially in poorly illuminated areas.

As for linear shot-encoding migration, we can extract common image gathers at fixed horizontal positions. If the dithering is kept small, mixed shot-encoding migration produces gathers that are comparable to linear shot-encoding migration. The limitation on the maximum delay used for encoding the wavefields reduces the moveout we observe when the velocity model is incorrect. Nonetheless, in simple geologic areas (for example, the sediment area in the Sigsbee model), mixed shot-encoding migration provides extra illumination despite the limited range of original take-off angles. The crosstalk noise in the prestack images is stronger in complex geologic areas (for example right above the salt body).

5 CONCLUSIONS

We design a hybrid encoding scheme, which we refer to as mixed shot-encoding, which combines the characteristics of linear and random shot-encoding in order to move across the

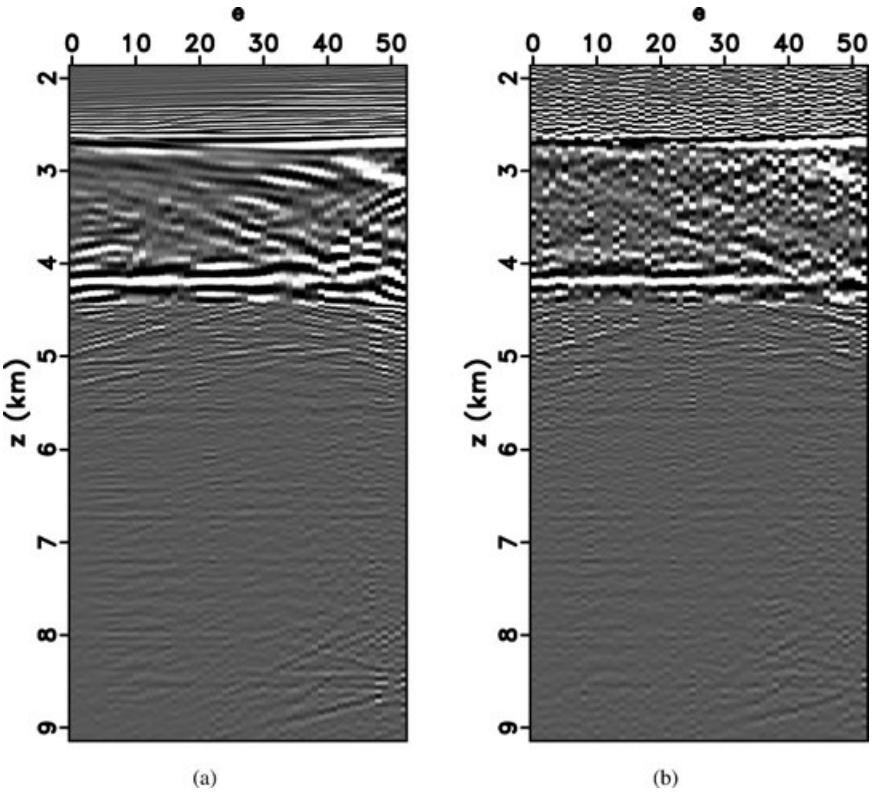


Figure 18 Common-image gather in the salt area ($x = 13.0$ km) obtained using (a) linear and (b) mixed shot-encoding migration with a 5% slower velocity model. The label *e* on the horizontal axis stands for 'experiments'; for linear shot-encoding migration, this axis represents the take-off angle of the source plane waves. The take-off angle range is from −15 to 15 degrees.

space defined by spatial bandwidth and crosstalk at a fixed computational cost. We analyse the behaviour of the shot coupling term and test mixed shot-encoding migration on the Sigsbee dataset, verifying the effectiveness of the algorithm. Dithering a planar wavefront, we increase the spatial bandwidth of the image and introduce weaker crosstalk noise compared to linear and random-shot encoding, respectively. We investigate the effects of the amount of dithering on the final image and verify that one can move smoothly from one extremum, linear shot-encoding, to the other extremum, random shot-encoding. The migrated image results are highly sensitive to dithering. Very little perturbation of the wavefront has a significant impact on the final image; in particular, the spatial bandwidth increases faster than crosstalk and a relatively small dithering allows one to recover spatial bandwidth without introducing strong artefacts.

The common-image gathers obtained by mixed shot-encoding migration have moveout features analogous to those obtained by linear shot-encoding migration. The crosstalk noise is much stronger in the prestack images and overwhelms reflection events in the common image gathers where the geology (and then the wavefield) is complex. The moveout is limited by the maximum delay applied during the encoding phase and this hampers the effectiveness of mixed shot-encoding for tomography applications that implement residual moveout picking and correction. In contrast, mixed-shot encoding supplies a complete structural image using a limited number of synthetic shot-gathers; a potential application is the picking of locations for computing common-image point gathers and for performing wave-equation migration velocity analysis. The direct application of mixed shot-encoding in the framework of the extended imaging condition and wave-equation migration velocity analysis is a second direction of investigation.

ACKNOWLEDGEMENTS

We would like to acknowledge the financial support provided by a research grant from Eni E&P and stimulating technical discussions with Clara Andreoletti and Nicola

Bienati. We would also like to thank Professor Biondo Biondi and an anonymous reviewer for their constructive comments that greatly improved the paper. The reproducible numeric examples in this paper use the Madagascar open-source software package freely available from http://www.reproducibility.org.

REFERENCES

Baysal E., Kosloff D.D. and Sherwood J.W.C., 1983. Reverse time migration. *Geophysics* **48**, 1514–1524.

Berkhout A.J., 2008. Changing the mindset in seismic acquisition. *The Leading Edge* **27**, 924–938.

Berkhout A.J., Verschuur D.J. and Blacquière G., 2009. Seismic imaging with incoherent wavefields. 79th SEG meeting, Houston, Texas, USA, Expanded Abstracts, 2894–2898.

Cazzola L., Pizzaferri L., Ratti L., Cardone G. and Bonomi e., 2004. An example of wavefield depth migration and Monte Carlo imaging in West Aafrica deep waters. 74th SEG meeting, Denver, Colorado, USA, Expanded Abstracts.

Claerbout J.F., 1985. Imaging the Earth's Interior. Blackwell Publishing.

Etgen J., 2005. How many angles do we really need for delayed-shot migration? 75th SEG meeting, Houston, Texas, USA, Expanded Abstracts, 1985–1988.

Lailly P., 1983. The seismic inverse problem as a sequence of before stack migrations. Conference on Inverse Scattering: Theory and Applications, pp. 206–220. SIAM.

Liu F., Hanson D.W., Whitmore N.D., Day R.S. and Stolt R.H., 2006. Toward a unified analysis for source plane wave migration. *Geophysics* **71**, S129–S139.

McMechan G.A., 1983. Migration by extrapolation of time-dependent boundary values. *Geophysical Prospecting* **31**, 413–420.

Morton S.A. and Ober C.C., 1998. Faster shot-record migration using phase encoding. 68th SEG meeting, New Orleans, Louisiana, USA, Expanded Abstracts.

Oppenheim A.V. and Schafer R.W., 1999. Discrete-time Signal Processing. Prentice Hall.

Paffenholz J., McLain B., Zaske J. and Keliher P., 2002. Subsalt multiple attenuation and imaging: Observations from the Sigsbee 2b synthetic dataset. 72nd SEG meeting, Salt lake City, Uttah, USA, Expanded Abstracts, 2122–2125.

Rickett J. and Sava P., 2002. Offset and angle-domain common image-point gathers for shot-profile migration. *Geophysics* **67**, 883–889.

Romero L.A., Ghiglia D.C., Ober C.C. and Morton S.A., 2000. Phase encoding of shot records in prestack migration. *Geophysics* **65**, 426–436.

Sava P.C. and Fomel S., 2003. Angle-domain common-image gathers by wavefield continuation methods. *Geophysics* **68**, 1065–1074.

Sava P.C. and Vasconcelos I., 2009. Extended common-image-point gathers for wave-equation migration. 71st EAGE meeting, Amsterdam, the Netherlands, Expanded Abstracts.

Soubaras R., 2006. Modulated-shot migration. 76th SEG meeting, New orleans, Lousiana, USA, Expanded Abstracts, 2430–2433.

Stolk C.C. and Symes W.W., 2004. Kinematic artifacts in prestack depth migration. *Geophysics* **69**, 562–575.

Stork C. and Kapoor J., 2004. How many P values do you want to migrate for delayed shot wave equation migration? 74th SEG meeting, Denver, Colorado, USA, Expanded Abstracts, 1041–1044.

Tang Y. and Biondi B., 2009. Least-squares migration/inversion of blended data. 79th SEG meeting, Houston, Texas, USA, Expanded Abstracts, 2859–2863.

Vasconcelos I., Sava P.C. and Douma H., 2010. Nonlinear extended images via image-domain interferometry. *Geophysics* **75**, SA105–SA115.

Verschuur D.J. and Berkhout A.J., 2009. Target-oriented, least-squares imaging of blended data. 79th SEG meeting, Houston, Texas, USA, Expanded Abstracts, 2889–2893.

Whitmore N., 1995. An imaging hierarchy for common-angle plane wave seismograms. PhD thesis, University of Tulsa.

Zhang Y., Sun J. and Gray S., 2007. Reverse-time migration: amplitude and implementation issues. 77th SEG meeting, San Antonio, Texas, USA, Expanded Abstracts, 2145–2148.

Zhang Y., Sun J., Notfors C., Gray S.H., Chernis L. and Young J., 2005. Delayed-shot 3D depth migration. *Geophysics* **70**, E21–E28.